Polymer Chemistry

PAPER

View Article Online
View Journal

Cite this: DOI: 10.1039/c8py01577e

Tailorable degradation of pH-responsive all polyether micelles *via* copolymerisation with varying acetal groups†

Jaeeun Song,‡[a] Eunbyul Hwang,‡[a] Yungyeong Lee,[a] L. Palanikumar,[a] Soo-Hyung Choi,[b] Ja-Hyoung Ryu[a] and Byeong-Su Kim*[c]

Smart drug delivery in a site-specific and time-controlled manner is critical for reducing the side effects of the drug while maximizing the therapeutic efficacy. Herein, we describe an efficient approach to control the degradation kinetics of polyether micelles under acidic conditions using random copolymers of functional epoxide monomers bearing different acetal groups. The amphiphilic block copolymers, poly (ethylene glycol)-*block*-poly(ethoxyethyl glycidyl ether-*co*-tetrahydropyranyl glycidyl ether)s (PEG-*b*-P (EEGE-*co*-TGE))s, are synthesized by the anionic ring-opening polymerisation of the pH-responsive novel epoxide monomers ethoxyethyl glycidyl ether (EEGE) and tetrahydropyranyl glycidyl ether (TGE) in varying ratios. The random block copolymers are carefully characterized by ^{1}H NMR, GPC, and DSC and the copolymerisation kinetics are evaluated using *in situ* ^{1}H NMR analysis. The critical micelle concentrations, loading efficiencies, and size distributions of the copolymer micelles show a saturation point over a critical TGE ratio. Interestingly, the degradation and subsequent release kinetics of the micelles under acidic conditions are remarkably different when the composition of the acetal groups is varied. The superior biocompatibility coupled with the highly tailorable release kinetics is anticipated to lead to a versatile platform for smart drug delivery systems.

Received 6th November 2018,
Accepted 14th December 2018

DOI: 10.1039/c8py01577e

rsc.li/polymers

1. Introduction

Over the past few decades, controlled drug delivery systems have been extensively studied by using nanocarriers such as polymeric micelles, liposomes, and nanoparticles.[1–3] In particular, polymeric micelles have generated significant interest as promising candidates to achieve desirable pharmacokinetic and biopharmaceutical outcomes for drug delivery. This is attributed to their distinctive features such as the enhanced solubility and circulation lifetime of therapeutics, as well as effective accumulation in tumours as a result of the enhanced permeability and retention (EPR) effect.[4,5]

Despite these advantages, there exist numerous challenges in terms of the location and time of drug delivery in a controlled manner. To meet this objective, the release kinetics have been studied at a targeted region in response to external stimuli such as pH, redox, light, and temperature.[6–8] In this regard, pH-responsive polymeric micelles are particularly interesting systems to selectively release the therapeutics by exploiting the various pH gradients existing in specific cellular compartments.[9] These polymers can be further expanded to other biological applications, including tumour targeted delivery of drugs, intracellular delivery of nucleic acids or proteins, treatment of inflammatory diseases, and oral administration.[10,11] In a time-controlled manner of intracellular nucleic acid or protein delivery, the rapid endosomal degradation of micelles is necessary for osmotic imbalance and release of the payload into the cytosol.[12,13] In contrast, oral administration and chronic diseases need a sustained release system to increase the drug bioavailability and decrease the fluctuations in drug concentrations.[14] Furthermore, it is particularly important to achieve an adequate amount of drug release for significantly improving the therapeutic efficacy with minimal side effects.

Several approaches have been adopted to develop pH-responsive polymers with imines, hydrazides, hydrazones, orthoesters, and acetal linkages.[15–17] Among them, the acetal

[a]*Department of Chemistry, Ulsan National Institute of Science and Technology (UNIST), Ulsan 44919, Republic of Korea*
[b]*Department of Chemical Engineering, Hongik University, Seoul 04066, Republic of Korea*
[c]*Department of Chemistry, Yonsei University, Seoul 03722, Republic of Korea. E-mail: bskim19@yonsei.ac.kr*

†Electronic supplementary information (ESI) available: GPC traces and DSC graphs of the synthesized polymers. ^{1}H NMR spectra of the *in situ* kinetics. Excitation spectra of pyrene for CMC measurement. Emission spectra of Nile Red. Excitation spectra of pyrene under pH 7.4 and pH 5.0 conditions. Cell images of *in vitro* FRET studies. See DOI: 10.1039/c8py01577e

‡These authors contributed equally to this work.

linkage is of particular interest because the degradation products formed upon cleavage are uncharged and potentially nontoxic. In addition, when the irreversible hydrolysis of acetals occurs, the degradation products are fully soluble, which is beneficial for enhanced renal clearance from the body.[18,19] For example, Kizhakkedathu and co-workers investigated the development of branched polyethers with structurally different ketal groups and studied their degradation kinetics.[20] More recently, De Geest and co-workers have studied the hydrolysis of paclitaxel–polymer conjugates with acetal linkages by controlling the hydrolysis kinetics.[21] They also synthesized acetal-based block copolymers and studied the degradation kinetics by changing the balance between hydrophilicity and hydrophobicity.[22] These studies suggest that the controlled release of active therapeutics with a wide timeframe is vital for developing a successful drug delivery system.

For biomedical applications of micelles, poly(ethylene glycol) (PEG) is the most commonly used hydrophilic block owing to its superior solubility, biocompatibility, and stealth effect.[23] Functional polyethers have recently attracted attention as an alternative to PEG because of their biocompatibility and other advantages such as various functionalities with controllable structures that can be synthesized in a facile manner.[24] To date, many novel epoxide monomers have been developed to synthesize polyethers with tunable physicochemical properties and functionalities.[25–30] As a notable example, we have recently reported a novel pH-responsive functional epoxide monomer, tetrahydropyranyl glycidyl ether (TGE), and its block copolymer, poly(ethylene glycol)-*block*-poly(tetrahydropyranyl glycidyl ether) (PEG-*b*-PTGE).[29] The self-assembly of the block copolymer into a micelle and its degradation kinetics under acidic conditions were thoroughly assessed and compared with those of other block copolymers containing the acyclic analogue, poly(ethylene glycol)-*block*-poly(ethoxyethyl glycidyl ether) (PEG-*b*-PEEGE).[31–33] Interestingly, the PEG-*b*-PTGE micelle showed a sustained release, whereas the PEG-*b*-PEEGE displayed a burst release under acidic conditions. However, it is still highly desirable to further tune the release kinetics to meet the demand for a drug delivery system with a wide window of release kinetics. Thus, our previous finding has prompted us to further develop a more general system using these two distinct monomers of TGE and EEGE.

Herein, we report the synthesis of pH-responsive random block copolymers based on EEGE and TGE monomers by anionic ring-opening polymerisation, using a *m*PEG macroinitiator to afford the block copolymers of PEG-*b*-P(EEGE-*co*-TGE) with varying ratios of EEGE and TGE monomers (Fig. 1 and Table 1). The random block copolymers consisted of a hydrophilic *m*PEG block ($M_{n,\ NMR}$ = 5900 g mol^{-1}) and a pH-responsive, hydrophobic block of poly(EEGE-*co*-TGE) with a tunable composition of the respective monomers. The random copolymers had a similar hydrophobic chain length while the compositional fraction of the TGE block varied from 0 to 100%. The main focus of this study is to examine the influence of the structure of the hydrophobic block on its self-assembly behaviour such as the critical micelle concentration (CMC), loading efficiency, and, most importantly, degradation kinetics with respect to the acetal ratio between the two monomers. The stimuli and time-specific release coupled with the biocompatibility of polyethers in our system is expected to offer a new means for sophisticated delivery of therapeutics in a controllable manner.

2. Results and discussion

Synthesis and characterisation of random copolymers

The pH-responsive monomers EEGE and TGE were synthesized in a facile, one-step procedure as reported previously.[29] Briefly, EEGE was synthesized from glycidol and ethyl vinyl ether,

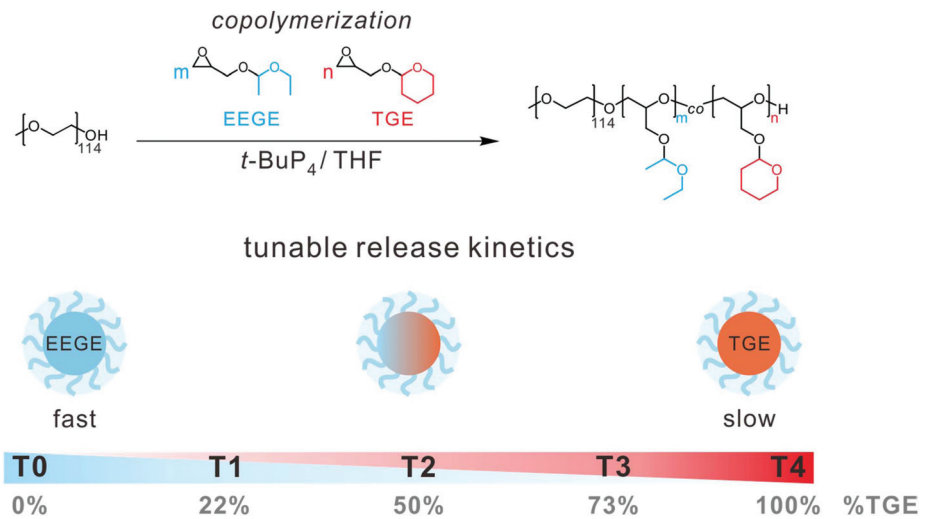

Fig. 1 Schematic representation of the copolymerisation of PEG_{114}-*b*-P(EEGE-*co*-TGE)$_{m/n}$ with a varying ratio of EEGE and TGE monomers (**T0–T4**) and the illustration of the tunable release kinetics from the corresponding micelles.

Table 1 Characterisation data of all synthesized polymers

Entry	Polymer composition[a]	F_{TGE}[a,c]	$M_{n,\ NMR}$[a] (g mol^{-1})	$M_{n,\ GPC}$[b] (g mol^{-1})	PDI[b]	T_g[d] (°C)	CMC[e] (mg L^{-1})
T0	PEG_{114}-*b*-P(EEGE-*co*-TGE)$_{27/0}$	0	9800	14 300	1.03	−58.9	76.7
T1	PEG_{114}-*b*-P(EEGE-*co*-TGE)$_{21/6}$	0.22	9900	14 100	1.03	−50.1	47.7
T2	PEG_{114}-*b*-P(EEGE-*co*-TGE)$_{14/14}$	0.50	10 100	13 500	1.03	−39.8	13.5
T3	PEG_{114}-*b*-P(EEGE-*co*-TGE)$_{7/19}$	0.73	9900	13 000	1.03	−29.5	10.9
T4	PEG_{114}-*b*-P(EEGE-*co*-TGE)$_{0/27}$	1	10 200	12 300	1.03	−18.2	10.9

[a] Determined *via* ^{1}H NMR spectroscopy in $CDCl_3$. [b] Measured using GPC measurement (DMF, RI signal, and PMMA standard). [c] Molar ratio of the TGE monomer in the hydrophobic block of PEG_{114}-*b*-P(EEGE-*co*-TGE)$_{m/n}$. [d] T_g was determined by differential scanning calorimetry (DSC) at a rate of 10 °C min^{-1}. [e] Critical micelle concentration (CMC) value was calculated from fluorescence spectroscopy using pyrene as a probe.

while TGE was synthesized from the reaction of glycidol and 3,4-dihydropyran in a high yield. Each monomer was purified by fractional distillation prior to polymerisation. Five random copolymers with varying compositional ratios of EEGE and TGE, PEG_{114}-*b*-P(EEGE-*co*-TGE)$_{m/n}$ (hereafter referred to as **T0–T4** in Table 1), were prepared *via* organic superbase *t*-BuP_4-catalyzed anionic ring-opening polymerisation using poly (ethylene glycol) monomethyl ether, *m*PEG ($M_{n,\ NMR}$ = 5900 g mol^{-1}), as a macroinitiator (Fig. 2). These copolymers were designed to afford a similar number of overall hydrophobic blocks during polymerisation, while the compositional fraction of the TGE block within the hydrophobic segment increases gradually from 0% for **T0** to 100% for **T4**.

The successful synthesis of **T0–T4** copolymers was confirmed by ^{1}H NMR, GPC, and DSC measurements (Fig. 2 and 3 and Fig. S1 in the ESI†). As shown in Fig. 2, the ^{1}H NMR spectra of the copolymers clearly indicated the characteristic proton peaks, including the methyl protons of *m*PEG (3.38 ppm), the polyether backbone (3.41–3.97 ppm), the tetrahydropyranyl protons (4.56–4.67 ppm and 1.44–1.91 ppm), and the ethoxyethyl protons (4.66–4.73 ppm and 1.15–1.33 ppm). The molecular weights (9800–10 200 g mol^{-1}) and the incorporation ratio of EEGE and TGE were determined based on the peak integral ratio between the methyl protons of *m*PEG and the methine protons of EEGE (4.66–4.73 ppm) and TGE (4.53–4.67 ppm) in the ^{1}H NMR spectra. Overall, the ratios of TGE over EEGE were successfully controlled from 0 to 100% in the hydrophobic block. It is worth noting that the change in the ratio of each methine proton was clearly demonstrated depending on the composition of the monomers. This indicated that the copolymerisation reaction using similar functional epoxide monomers successfully afforded block copolymers that were *exclusively* composed of a polyether backbone.

In concert with the ^{1}H NMR data, the GPC results of the copolymers indicated monomodal distributions with narrow

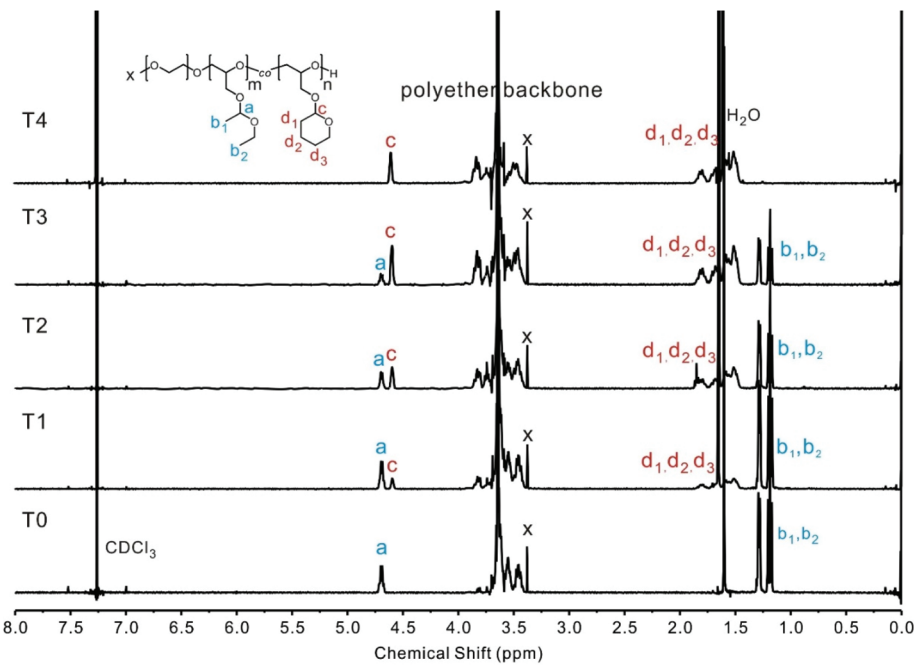

Fig. 2 ^{1}H NMR spectra of the PEG_{114}-*b*-P(EEGE-*co*-TGE)$_{m/n}$ copolymers **T0–T4**. All spectra were recorded in $CDCl_3$. The gradual changes in the methine peaks of *a* and *c* arising from each monomer of the EEGE (peak *a*) and TGE (peak *c*) block can be clearly observed.

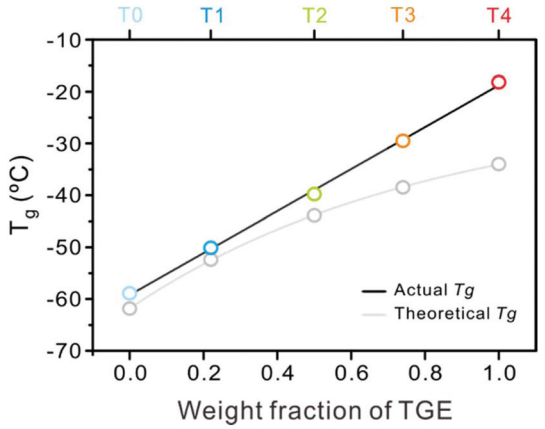

Fig. 3 Glass transition temperature (T_g) of PEG_{114}-*b*-P(EEGE-*co*-TGE)$_{m/n}$ copolymers as a function of the weight fraction of the TGE monomer. The T_g was determined by DSC at a rate of 10 °C min^{-1}. The theoretical T_g value was calculated by the Fox equation.

polydispersity indexes (M_w/M_n = 1.03) in all cases with reference to the poly(methyl methacrylate) (PMMA) standard in DMF (Table 1 and see Fig. S1 in the ESI†). The traces of all the copolymers shifted to a higher molecular weight region as compared to that from the *m*PEG macroinitiator. Interestingly, we observed that the $M_{n,\ GPC}$ values of the copolymers tended to decrease with increasing ratio of the TGE monomer, regardless of the value calculated by ^{1}H NMR. This tendency was likely due to the increased hydrophobicity of the TGE block, which suppressed the hydrodynamic volume of the copolymers in DMF.[34]

The successful copolymerisation was further assessed by measuring the glass transition temperature (T_g) of the copolymers using differential scanning calorimetry (DSC) (Fig. 3 and Fig. S2†). Interestingly, all copolymers exhibited a single T_g, which indicated that the product was a random copolymer with EEGE and TGE monomers, again confirming that the block copolymers were *exclusively* comprised of the polyether backbone (Fig. S2†). As expected, the T_g of the copolymers increased with increasing TGE ratio in the copolymers. When the copolymer was synthesized with only the EEGE unit, the T_g of the copolymer **T0** was found to be −59.8 °C, similar to the reported value of the PEEGE homopolymer, −59.0 °C.[35] As the fraction of the TGE monomer was increased further, the T_g of the copolymers increased linearly up to −18.2 °C (**T4**). Using the Fox equation to fit the experimental T_g values with the theoretical ones, a positive deviation attributable to the bulky side chain of TGE monomers was obtained (Fig. 3).[36] As the weight fraction of TGE in the copolymers increased, the deviation in T_g also increased, as reported similarly in other literature; for example, Moore *et al.* observed a similar trend in the T_g values of styrene/maleic anhydride copolymers, which displayed a linear increase in T_g with increasing amount of maleic anhydride.[37]

To observe the microstructure of the PEG_{114}-*b*-P(EEGE-*co*-TGE)$_{m/n}$ copolymers, we monitored the copolymerisation kinetics of EEGE and TGE. The total conversion ratio of both EEGE and TGE monomers was plotted against the overall monomer conversion ratio, as shown in Fig. 4. The monomer conversion was observed for 12 h using ^{1}H NMR and calculated from the integration values of the methine protons of each monomer against the signal from the methyl proton of the *m*PEG macroinitiator, which remained constant during polymerisation. Based on the non-terminal model of chain copolymerisation developed by Lynd and co-workers,[38] we found that the random copolymerisation of EEGE and TGE had reactivity ratios of r_{EEGE} = 1.49 ± 0.01 and r_{TGE} = 0.69 ± 0.01 with a product of $r_{EEGE} \cdot r_{TGE}$ = 1.03, yielding almost ideal copolymeri-

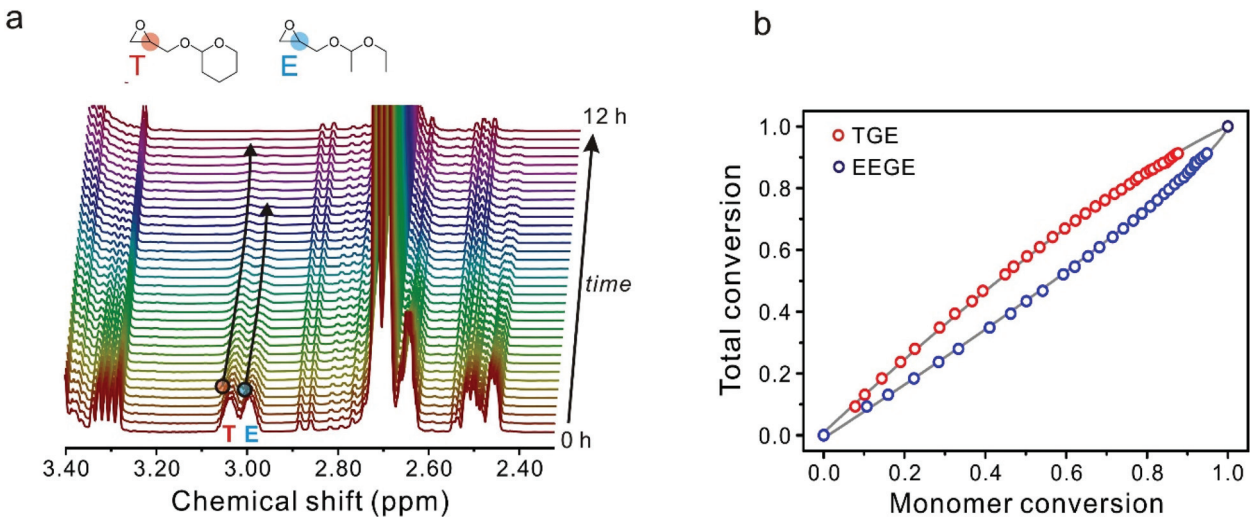

Fig. 4 (a) *In situ* monitoring of the copolymerisation kinetics of EEGE and TGE (initial monomer ratio of 1 : 1) to afford PEG_{114}-*b*-P(EEGE-*co*-TGE)$_{14/14}$. The ^{1}H NMR spectra were recorded every 30 min for 12 h (THF-d_8, 400 MHz, 25 °C). (b) Total conversion *versus* monomer conversion for the copolymerisation of TGE (red circle) and EEGE (blue circle), as determined by the *in situ* ^{1}H NMR experiment.

sation. The slightly lower reactivity of the TGE monomers could have originated from the sterically hindered cyclic monomer structure as compared to the acyclic EEGE monomer. Although this kinetic experiment showed that there was a small gradient of the microstructure in the copolymers, it should be noted that polymerisation was performed in bulk within an NMR tube.

Self-assembly behaviour

The CMC of a polymer is a crucial factor that indicates its ability to self-assemble and the stability of its micelle in solution. Therefore, we investigated the CMC values of the synthesized copolymers by using pyrene as a fluorescent probe.[39,40] Following the encapsulation of pyrene into the hydrophobic core of the micelles above a certain concentration of the polymer, a dramatic increase in the intensity and a red shift were observed in the excitation spectra. The relative ratios of peak intensities at 339 nm and 332 nm (I_{339}/I_{332}) were plotted as a function of the concentrations of the respective polymers (see Fig. S3–S7† for the recorded spectra and the corresponding plot to determine the CMC values). The CMC values of **T0–T4** polymers were determined to be 76.7 (**T0**), 47.7 (**T1**), 13.5 (**T2**), 10.9 (**T3**), and 10.9 mg L^{-1} (**T4**), respectively, as shown in Fig. S8.† When the copolymer was synthesized with only EEGE (**T0**), the CMC was higher than that of the polymer with only TGE (**T4**). As similarly reported in the study of the effect of side-chain hydrophobicity on CMC,[41] the CMC values of the copolymers decreased upon the increase of the hydrophobicity by incorporating the more hydrophobic TGE monomer. However, it remained constant over a certain TGE ratio (corresponding to **T2**). This trend suggests that incorporating a certain TGE monomer ratio was enough to reduce the free energy of micellisation and led to a sufficient driving force for self-assembly.

The size of the micelles is also critical to their circulation time and distribution in the body.[42] The distribution of the hydrodynamic radius (R_h) of the micelles at 32 °C was characterized by dynamic light scattering (DLS) as shown in Fig. 5. All block copolymer micelles show a hydrodynamic radius (R_h) between 14 and 18 nm with a relatively narrow polydispersity less than 0.15 at 32 °C.

Many poly(glycidyl ether) polymers with a pendant side chain exhibited lower critical solution temperature (LCST)-type thermoresponsive behaviour, and their phase transition temperature is highly dependent on the structure of the side chain.[43,44] The fraction of EEGE monomers in the hydrophobic block can control the transition temperature of micellisation as indicated by the scattered intensity of DLS (Fig. S9†). At lower temperature, the scattered intensity is relatively low indicating that block copolymers are soluble in water. A gradual increase in the scattered intensity, however, reflects the formation of micelles. Since the EEGE monomer is more hydrophilic than the TGE monomer,[29] the fraction of EEGE decreases as the micelle transition temperature becomes lower, and thus the micelles become more well defined with a more hydrophobic core block near room temperature.

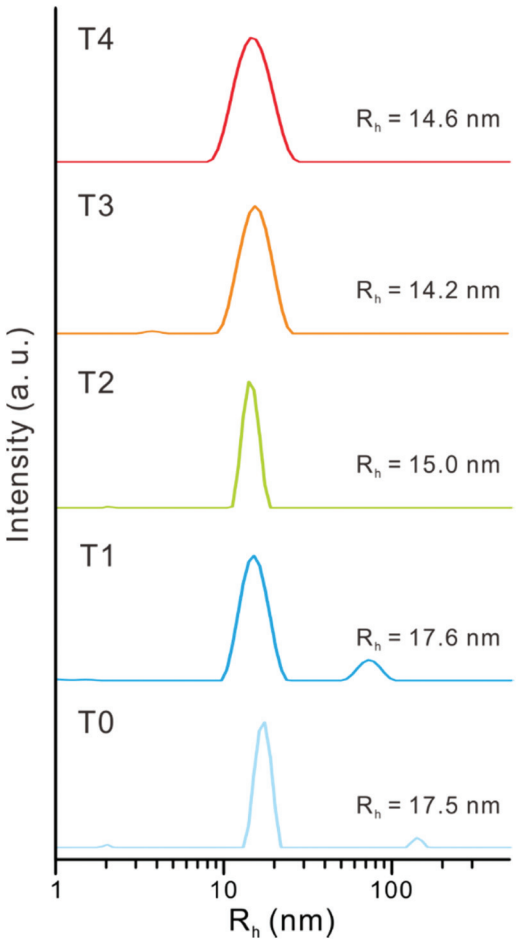

Fig. 5 Distribution of the hydrodynamic radius (R_h) of the **T0–T4** micelles in water at 32 °C as measured by DLS.

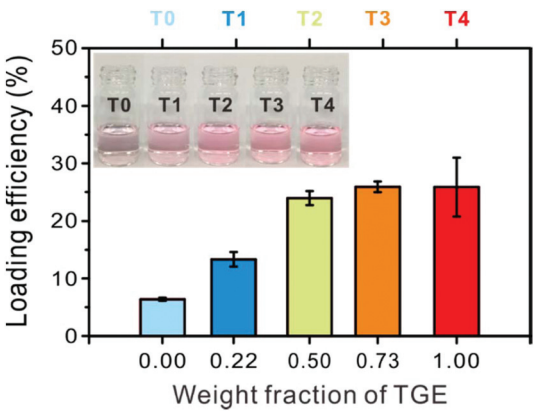

Fig. 6 Loading efficiency of Nile Red in all copolymer micelles (average of three independent experiments). The inset shows the suspensions of micelles containing Nile Red. The polymer concentration was set to 1.0 mg mL^{-1}.

As a nanoscale carrier, the drug loading efficiency was also investigated by encapsulating the model hydrophobic dye, Nile Red, within the micelles. As shown in Fig. 6, the Nile Red

loading efficiencies of the micelles prepared from the copolymers were 6.4 (**T0**), 13.3 (**T1**), 23.9 (**T2**), 25.9 (**T3**), and 25.9% (**T4**). The loading efficiencies of the micelles increased with increasing ratio of the incorporated TGE monomer and were saturated over **T2**, in accordance with the CMC values. Taken together, it was concluded that the incorporation of the hydrophobic, cyclic TGE monomer provided a sufficient driving force for the formation of micelles with enhanced stabilities and loading capacities.

Degradation kinetics in acidic environments

For stimuli-responsive drug delivery systems, pH-responsive micelles have been actively studied because of the wide range of pH changes in different cellular compartments.[45–48] In our system, the degradation of the copolymers takes place as a result of the dissociation of acetal linkages of the TGE and EEGE monomers under acidic conditions. Furthermore, it is reasonable to expect that the degradation kinetics would be controlled by the fraction of each monomer. To gain an insight into the pH sensitivity of micelles, we studied the pH-triggered release of encapsulated pyrene. The ratio of fluorescence intensity at 339 nm and 332 nm (I_{339}/I_{332}) was normalized and plotted as a function of time (Fig. 7). We first investigated the degradation of micelles at pH 7.4 by monitoring the change of the I_{339}/I_{332} ratio of pyrene in the excitation spectra (Fig. 7b and Fig. S11†). The I_{339}/I_{332} value of pyrene for the **T0–T4** micelles did not change significantly, suggesting that the micelles were stable under neutral conditions. However, upon switching to pH 5.0, the intensity of the fluorescence excitation spectra was shifted and decreased with time as the encapsulated pyrene was released (Fig. 7c and Fig. S12†). The rate of pyrene release was slow for the copolymers that included a higher percentage of the TGE monomer. For example, most of the pyrene was released within 1 day for **T0**, while 50% of the loaded pyrene was released in 1 day, 3 days, and 5 days for **T1**, **T2**, and **T3**, respectively. It is worth noting that the micelle from the **T4** copolymer displayed the longest release time, suppressing the initial burst and extending the release over two weeks.

These extended release profiles indicate that the incorporation of the TGE monomers is one of the tools to control the hydrophobicity and the degree of packing of the core, which can reduce the protonation and subsequent hydrolysis of the acetal linkages. Moreover, these observations support the conclusion that the degradation kinetics of the micelles can be easily tuned by using different types of acetal groups and controlling the ratio of the acetal groups.

In vitro FRET study

The loaded therapeutics in the micelles are transferred to the plasma membrane, where they either undergo endocytosis or diffuse to the intracellular organelles in a target cell.[49,50] Thus,

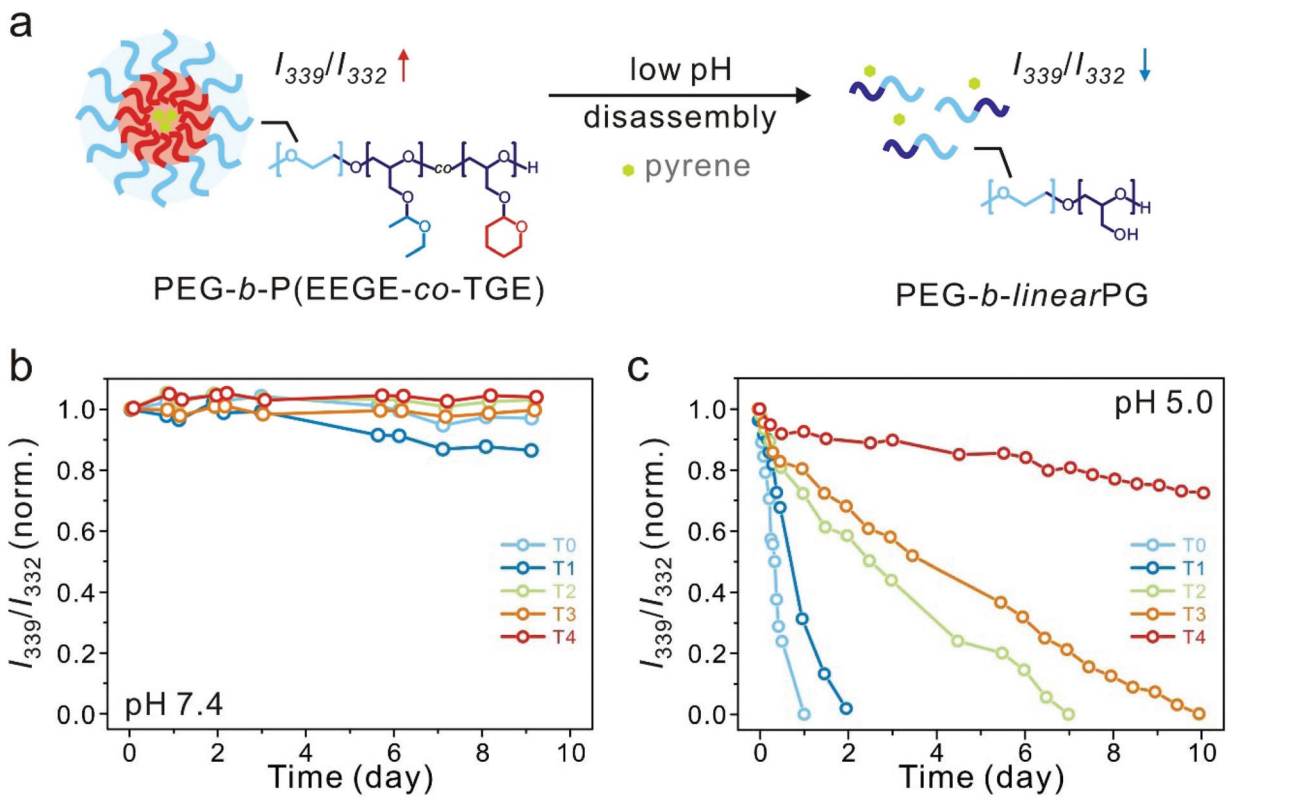

Fig. 7 (a) Schematic illustration of the release of the encapsulated model drug, pyrene. (b, c) Release profile of pyrene from the degradation of copolymer micelles over time at (b) pH 7.4 and (c) pH 5.0. The percentage of degradation was plotted using the I_{339}/I_{332} values of pyrene calculated from the excitation spectra.

it is necessary to elucidate the release of therapeutics in a biological system and evaluate the cellular uptake to achieve successful intracellular drug delivery in a controlled manner. To investigate the release of therapeutics from the micelles, the Förster resonance energy transfer (FRET)-based method was used in this study, as previously reported.[51] The FRET-based method is useful to assess non-covalent guest exchange dynamics in an aqueous solution. For example, Thayumanavan and co-workers evaluated the encapsulation stability of nanogels using the FRET of non-covalently capsulated dyes, dioctadecyloxacarbocyanine perchlorate (DiO)/1,1′-dioctadecyl-3,3,3′,3′-tetramethylindocarbocyanine perchlorate (DiI).[52–54] The FRET pair comprised of the donor, DiO, and the acceptor, DiI, was loaded into the micelle. When both FRET pair molecules were encapsulated inside the micelle and the DiO donor was excited at 488 nm, energy transfer occurred because of the proximity of the molecules within the micelle, which resulted in the emission of the DiI acceptor at 564 nm (red colour). In contrast, when the micelles disintegrated and the dyes were released, the FRET molecules diffused apart and eliminated the FRET effect, which resulted in the emission of the DiO donor at 501 nm (green colour).

The FRET dye-loaded micelles were prepared as described in the Experimental section. Here, we chose the **T2**, **T3**, and **T4** micelles because of the insufficient loading efficiency of the **T0** and **T1** micelles. The HeLa (human epithelial carcinoma cancer) cells were incubated with the FRET dye-loaded micelles for different time periods and visualized by excitation at 488 nm (Fig. 8 and Fig. S13–S15†). It was found that the release of FRET dyes and the cellular uptake rate became slower as the TGE monomer fraction was increased. As shown in Fig. 8, the **T2** micelles showed strong yellow fluorescence from the overlaid green (DiO) and red (DiI) signals on the plasma membrane for the cells incubated after 30 min and the dyes were then internalized into the cytoplasm after 1 h. This indicated that the **T2** micelles were readily dissociated under biological conditions and could deliver therapeutics rapidly into the cytoplasm. The internalisation of the **T3** micelles could be observed by weak red fluorescence in the cytoplasm without the yellow fluorescence on the cell membrane after 1 h. The dyes in the **T3** micelles were released on the cell membrane and in the cytoplasm after 2 h, which was slower than that in the **T2** micelles. Notably, for the **T4** micelles, there was strong red fluorescence in the cytoplasm without the yellow fluorescence on the cell membrane even after 3 h, indicating that there was no structural degradation of the micelles. The dyes were released after 4 h (see Fig. 8 and Fig. S15†), suggesting that the **T4** micelles were capable of being internalized into the cytoplasm without the premature release of the dyes on the cell membrane. This indicated that the micelles retained their payload with integrity while entering the cytoplasm as the fraction of TGE monomers was increased. The difference in the release kinetics and the cellular uptake rate between the **T2**, **T3**, and **T4** micelles could be attributed to two factors. One is the increased stability of the micelles as the hydrophobicity of the core was increased by the hydrophobic TGE monomers. The other factor is due to the close packing and increased torsional strain with increasing fraction of the

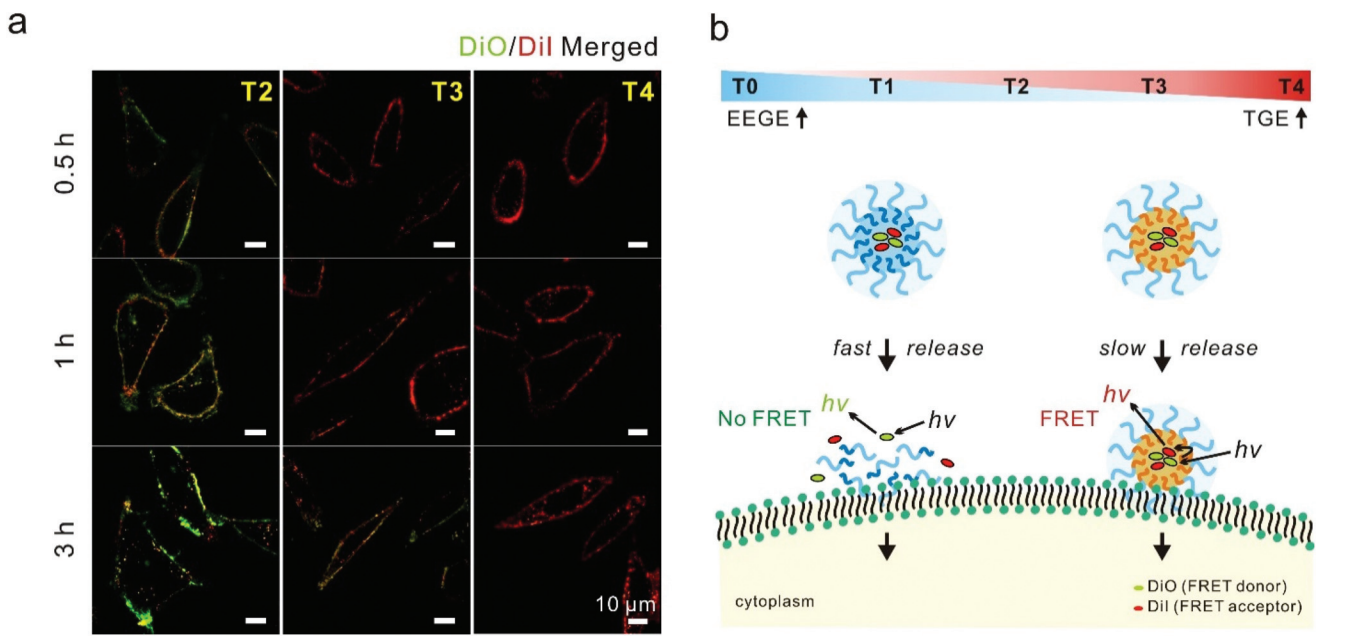

Fig. 8 (a) *In vitro* FRET studies for the **T2**, **T3**, and **T4** micelles after incubation in HeLa cells for different time periods. The green and red colours represent the DiO and DiI signals, respectively, and the yellow colour indicates the overlapped signals of both FRET dyes. The **T0** and **T1** micelles are not included because of the low loading efficiency. The excitation and emission wavelengths for DiO were 488 and 535 nm, and that for DiI were set to 543 and 620 nm, respectively. Scale bars: 10 μm. See Fig. S13–S15† for all obtained images. (b) Schematic illustration of the different release mechanisms for the micelles.

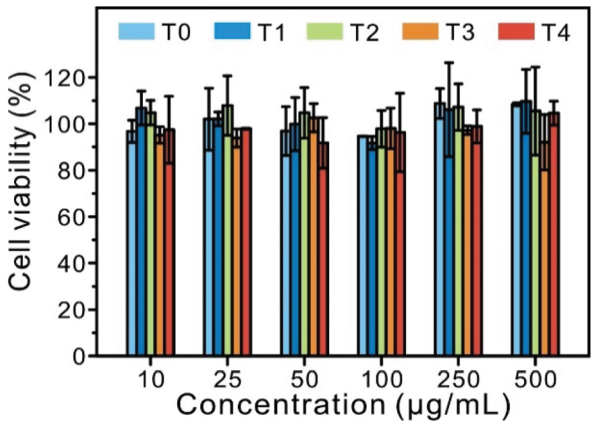

Fig. 9 *In vitro* cell viability assay of all copolymer micelles prepared from **T0–T4** as determined by the MTT assay using HeLa cells. The values are reported with an average of five independent experiments.

TGE monomer, which reduced the direct interaction with the membrane lipid bilayer. In addition, the discrepancy in terms of the release kinetics of the FRET-based assay compared to that performed in the buffer can be attributed to the presence of albumin and other salts in the cellular environments and the use of a relatively lower concentration of polymers.

Cell viability assay

Finally, we evaluated the cellular viability of all micelles to evaluate their potential applicability as drug delivery carriers. Each micelle was treated with HeLa cells to investigate their viability using the MTT assay. As shown in Fig. 9, the cell viability after treating the micelle solutions of varying concentrations was nearly 100%, even at a high concentration of 250 μg mL^{-1}. However, the cell viability of the **T3** micelle (micelles having a longer hydrophobic chain) decreased slightly at a concentration of 500 μg mL^{-1}. This could be explained by the fact that long hydrophobic chains likely have a negative effect on biocompatibility. Consequently, micelle stability and biocompatibility should be carefully optimized to achieve the best performance as drug delivery carriers. As Xia *et al.* have recently demonstrated that the residual phosphazene base was responsible for cytotoxicity,[55] we removed the residual base completely from the polymers as evidenced by the ^{1}H NMR spectra (Fig. S16 in the ESI†).

3. Conclusion

In summary, we developed novel pH-responsive block copolymer micelles to control the release kinetics of therapeutics in a site-specific and time-controlled manner. A series of block copolymers, PEG-*b*-P(EEGE-*co*-TGE), were synthesized by anionic ring-opening polymerisation by controlling the ratio of the two functional epoxide monomers, namely, EEGE and TGE, with acyclic and cyclic acetal moieties. The random copolymerisation was successfully characterized by ^{1}H NMR, GPC, and DSC measurements, and the copolymerisation kinetics between the two monomers were further studied by *in situ* ^{1}H NMR analysis. The CMC values, loading efficiencies, and degradation kinetics of the micelles prepared from the series of PEG-*b*-P(EEGE-*co*-TGE) copolymers were controlled by varying the fraction of the TGE monomers with the cyclic analogue. In particular, the micelles of PEG-*b*-P(EEGE-*co*-TGE) copolymers showed highly tunable release kinetics under mild acidic conditions and biological conditions, which were attributed to the changed hydrophobicity and degree of packing arising from the cyclic TGE side chains. The tunable properties and high biocompatibility clearly demonstrate the immense potential of these functional polymer micelles in drug delivery. We anticipate that the novel approach developed in this study will broaden the smart drug delivery system and offer promising candidates for biomaterials and biomedical applications.

4. Experimental section

Materials

All reagents and solvents were purchased from Sigma-Aldrich and Acros and used as received unless otherwise stated. Dry dichloromethane and THF were obtained from a solvent drying system and used immediately thereafter. All deuterated NMR solvents such as $CDCl_3$ and THF-d_8 were purchased from Cambridge Isotope Laboratories.

Characterisation

^{1}H-NMR (400 MHz) and ^{13}C-NMR spectra (100 MHz) were recorded using a 400-MR DD2 spectrometer. All spectra were recorded in ppm units with tetramethylsilane (TMS) as an internal standard in the deuterated solvents $CDCl_3$ and THF-d_8. GPC measurements (Agilent 1200 series) were performed in DMF as an eluent at 25 °C with a flow rate of 1.0 mL min^{-1} using a refractive index (RI) detector. Standard poly(methyl methacrylate) samples were used for calibration to determine the number- and weight-averaged molecular weight (M_n and M_w). Differential scanning calorimetry (DSC) was carried out under a nitrogen atmosphere using a differential scanning calorimeter (Q200 model, TA Instruments) in the temperature range of −80 °C to 65 °C and at a heating rate of 10 K min^{-1}. The CMC measurements, the loading efficiency measurement of Nile Red, and the FRET tests were carried out using a fluorometer (RF-6000, Shimadzu). The size distribution analysis of the micelles was performed by dynamic light scattering (DLS, BI-APD, Brookhaven Instrument) at 90° and 30°.

Synthesis of PEG-*b*-P(EEGE-*co*-TGE) block copolymers, T2

Random copolymer synthesis was conducted using poly(ethylene glycol)methylether (*m*PEG) as a macroinitiator. *m*PEG (0.50 g, 0.10 mmol) was placed in a flask under an argon flow. Toluene (3.47 mL) was added to the flask and the mixture was stirred for 30 min at 60 °C. After cooling to room temperature, 0.13 mL of *t*-Bu-P_4 in *n*-hexane (0.80 M, 0.10 mmol) was added to the solution. Next, TGE (0.24 g, 1.5 mmol) and EEGE

(0.22 g, 1.5 mmol) were added together to the solution dropwise over 6 h using a syringe pump. After stirring at room temperature for 24 h, polymerisation was terminated by the addition of benzoic acid. After precipitation in hexane, the reaction mixture was passed through a pad of alumina with THF. The solution was evaporated to dryness to give poly(ethylene glycol)-*b*-poly(ethoxyethyl glycidyl ether-*co*-tetrahydropyranyl glycidyl ether), PEG-*b*-P(EEGE-*co*-TGE) (0.71 g). Yield: 70.5%. The M_n of PEG-*b*-P(EEGE-*co*-TGE)$_{14/14}$ (polymer 3, **T2** in Table 1) was determined to be 10 100 g mol^{-1}, as calculated from the NMR data (see Fig. 2) using the following equation: number of repeating units (TGE) = 4.71 (integration value) × 3 (number of protons of the methyl of *m*PEG) = 14; number of repeating units (EEGE) = 4.58 (integration value) × 3 (number of protons of the methyl of *m*PEG) = 14; and M_n = 158.20 (molecular weight of the TGE monomer) × 14 + 146.19 (molecular weight of the EEGE monomer) × 14 + 5900 (molecular weight of the *m*PEG macroinitiator) = 10 161.5 g mol^{-1}. Considering the error range of NMR integration, we used 10 100 g mol^{-1} as the M_n value of PEG-*b*-P(EEGE-*co*-TGE) (polymer 3, **T2** in Table 1). The ratio of the two monomers was varied to synthesize different copolymers (**T0–T4**). ^{1}H NMR (400 MHz, chloroform-*d*) δ 4.69 (d, J = 5.6 Hz, 1H, CH), 4.60 (s, 1H, CH), 3.97–3.42 (m, 51H, backbone), 1.91–1.44 (m, 15H, $CH_2CH_2CH_2$, water), 1.30–1.26 (m, 3H, CH_3), and 1.19 (t, J = 7.1 Hz, 3H, CH_3).

Micelle formation and characterisation

A 5.0 mg sample of the PEG-*b*-P(EEGE-*co*-TGE) copolymer was dissolved in 200 μL of DMF, after which 4.8 mL of water was added dropwise over 1 h using a syringe pump to form micelles. After stirring overnight to stabilize the micelles, the solution was dialyzed against deionized water for 2 days to exchange the residual DMF. The solution was then filtered through a 0.45 μm syringe filter (PVDF-d) before DLS analysis. DLS measurements were performed using a nano particle analyzer (SZ-100, HORIBA) equipped with a solid-state laser (λ = 532 nm). The intensity autocorrelation function was measured at an angle of 90 °C, and analysed by the cumulant method where the average decay rate (Γ) and the second cumulant (μ^2) were employed to determine the mean hydrodynamic radius (R_h) and its polydispersity (PDI = μ^2/Γ^2).[56]

Pyrene fluorescence measurements and CMC studies

A series of polymer solutions in DMF at various concentrations were prepared. A 10 μL solution of pyrene (5.2 mg L^{-1} in DMF) was added to the solution of the PEG-*b*-P(EEGE-*co*-TGE) copolymer and the mixture was stirred for 30 min at room temperature. Subsequently, a total of 5 mL of DI water was added to the solution at a rate of 0.5 mL min^{-1} using a syringe pump. The solution was left to equilibrate overnight. The fluorescence of each pyrene-containing polymer micelle solution (having different concentrations) was measured at an emission wavelength of 372 nm using a fluorimeter (RF-6000, Shimadzu) through a 1 × 1 cm quartz cell. The following parameters were chosen: emission wavelength = 372 nm, excitation wavelength range = 360–372 nm, and data interval = 0.5 nm. The ratio of the fluorescence intensities at wavelengths of 339 and 332 nm was plotted *versus* the polymer concentrations and the CMC was determined from the inflection point.

Encapsulation efficiency

The encapsulation efficiency (EE) of the micelles was calculated from the fluorimeter analysis results as follows. A 0.10 mL solution of Nile Red (50 μg mL^{-1} in acetone) was added to a solution of the PEG-*b*-P(EEGE-*co*-TGE) copolymer (5 mg) in acetone (0.10 mL) and the mixture was stirred for 30 min at room temperature. The loading percentage of Nile Red to the polymer was 0.1 wt%. A total of 5 mL of deionized water was then added to the solution at a rate of 0.5 mL min^{-1} using a syringe pump. The solution was then left to equilibrate overnight allowing the acetone to evaporate with the lid open. After filtration using a 0.45 μm syringe filter, the solution was lyophilized and redissolved in acetone. The amount of Nile Red loaded in the micelles was determined by measurements using a fluorometer (RF-6000, Shimadzu) through a 1 × 1 cm quartz cell as follows:

$$\mathrm{EE}(\%) = \frac{\text{concentration of drug measured}}{\text{concentration of drug added}} \times 100.$$

The following parameters were chosen: excitation wavelength = 480 nm, emission wavelength range = 500–800 nm, and data interval = 0.5 nm.

Degradation kinetic study

For degradation kinetic studies, a buffer solution at pH 5.0 was prepared using sodium acetate/acetic acid and a pyrene-containing polymeric micelle solution was prepared according to the procedure described in the CMC study above. Then, 0.10 mL of the pyrene-containing micelle solution was slowly added to 0.9 mL of the buffer solution and the changes in the excitation spectra were recorded.

In vitro imaging of cells incubated with DiO/DiI loaded micelles

HeLa cells (purchased from the Korea Cell Line Bank) were cultured in Dulbecco's modified Eagle's medium (DMEM) supplemented with 10% fetal bovine serum (FBS) and 1% penicillin–streptomycin (Invitrogen Life Technologies, Korea). The cells were maintained under a humid atmosphere containing 5% CO_2 at 37 °C, and the medium was changed every other day. The cells were cultured on eight-well Lab-Tek glass chamber slides (Thermo Fisher Scientific, Korea), treated with 3,3′-dioctadecyloxacarbocyanine perchlorate (DiO)/1,1′-dioctadecyl-3,3,3′,3′-tetramethylindo carbocyanine perchlorate (DiI) co-loaded micelles at a concentration of 0.5 μg mL^{-1}, and incubated at different time points. The images were captured using an Olympus confocal laser scanning microscope model FV1000 with the excitation filter set to 473 nm.

In vitro cell cytotoxicity

Cytotoxicity tests were carried out to investigate the toxicity of micelles and their ability to act as drug delivery carriers by a modified thiazolyl blue tetrazolium bromide (MTT) assay. Briefly, HeLa cells were grown in a 96-well plate with a growth medium comprising DMEM, 10% FBS, and 1% penicillin–streptomycin at a density of 3×10^4 cells per well. After incubating for 24 h under a humidified atmosphere of 95% air/5% CO_2 for stabilizing the cells, the HeLa cells were treated with each micelle type. After 24 h, 10 μL of MTT was added in each well (final concentration of 0.5 mg mL^{-1}), and incubated for 3 h. Subsequently, the culture medium was removed and 100 μL of DMSO was added to each cell well to dissolve the remaining MTT reagent. Finally, the plates were gently agitated for 15 min at room temperature to dissolve the MTT in DMSO. The absorbance was measured at a wavelength of 540 nm using a reference of 620 nm.

Conflicts of interest

There are no conflicts to declare.

Acknowledgements

This work was supported by the National Research Foundation of Korea (NRF-2017R1A2B3012148).

References

1 H. Otsuka, Y. Nagasaki and K. Kataoka, *Adv. Drug Delivery Rev.*, 2003, **55**, 403–419.
2 M. Murakami, H. Cabral, Y. Matsumoto, S. Wu, M. R. Kano, T. Yamori, N. Nishiyama and K. Kataoka, *Sci. Transl. Med.*, 2011, **3**, 64ra2.
3 G. Pillai, *SOJ Pharm. Pharm. Sci.*, 2014, **1**, 1–13.
4 S. S. Kulthe, Y. M. Choudhari, N. N. Inamdar and V. Mourya, *Des. Monomers Polym.*, 2012, **15**, 465–521.
5 Z. Ahmad, A. Shah, M. Siddiq and H.-B. Kraatz, *RSC Adv.*, 2014, **4**, 17028–17038.
6 N. Kamaly, B. Yameen, J. Wu and O. C. Farokhzad, *Chem. Rev.*, 2016, **116**, 2602–2663.
7 C. Oerlemans, W. Bult, M. Bos, G. Storm, J. F. W. Nijsen and W. E. Hennink, *Pharm. Res.*, 2010, **27**, 2569–2589.
8 F. Meng, Z. Zhong and J. Feijen, *Biomacromolecules*, 2009, **10**, 197–209.
9 Y. Liu, W. Wang, J. Yang, C. Zhou and J. Sun, *Asian J. Pharm. Sci.*, 2013, **8**, 159–167.
10 C.-Y. Sun, S. Shen, C.-F. Xu, H.-J. Li, Y. Liu, Z.-T. Cao, X.-Z. Yang, J.-X. Xia and J. Wang, *J. Am. Chem. Soc.*, 2015, **137**, 15217–15224.
11 J. Ren, Y. Zhang, J. Zhang, H. Gao, G. Liu, R. Ma, Y. An, D. Kong and L. Shi, *Biomacromolecules*, 2013, **14**, 3434–3443.
12 Y. Hu, T. Litwin, A. R. Nagaraja, B. Kwong, J. Katz, N. Watson and D. J. Irvine, *Nano Lett.*, 2007, **7**, 3056–3064.
13 M. Stubbs, P. M. McSheehy, J. R. Griffiths and C. L. Bashford, *Mol. Med. Today*, 2000, **6**, 15–19.
14 Y. Zhang, J. Chen, G. Zhang, J. Lu, H. Yan and K. Liu, *React. Funct. Polym.*, 2012, **72**, 359–364.
15 Y. Jin, L. Song, Y. Su, L. Zhu, Y. Pang, F. Qiu, G. Tong, D. Yan, B. Zhu and X. Zhu, *Biomacromolecules*, 2011, **12**, 3460–3468.
16 A. J. M. D'Souza and E. M. Topp, *J. Pharm. Sci.*, 2004, **93**, 1962–1979.
17 R. G. J. Heller, J. Barr, S. Y. Ng, H.-R. Shen, K. Schwach-Abdellaoui, S. Einmahl and A. Rothen-Weinhold, *Eur. J. Pharm. Biopharm.*, 2000, **50**, 121–128.
18 E. R. Gillies, A. P. Goodwin and J. M. J. Fréchet, *Bioconjugate Chem.*, 2004, **15**, 1254–1263.
19 M. J. Heffernan and N. Murthy, *Bioconjugate Chem.*, 2005, **16**, 1340–1342.
20 R. A. Shenoi, J. K. Narayanannair, J. L. Hamilton, B. F. L. Lai, S. Horte, R. K. Kainthan, J. P. Varghese, K. G. Rajeev, M. Manoharan and J. N. Kizhakkedathu, *J. Am. Chem. Soc.*, 2012, **134**, 14945–14957.
21 B. Louage, M. J. van Steenbergen, L. Nuhn, M. D. P. Risseeuw, I. Karalic, J. Winne, S. Van Calenbergh, W. E. Hennink and B. G. De Geest, *ACS Macro Lett.*, 2017, **6**, 272–276.
22 B. Louage, Q. Zhang, N. Vanparijs, L. Voorhaar, S. Vande Casteele, Y. Shi, W. E. Hennink, J. Van Bocxlaer, R. Hoogenboom and B. G. De Geest, *Biomacromolecules*, 2015, **16**, 336–350.
23 J. Herzberger, K. Niederer, H. Pohlit, J. Seiwert, M. Worm, F. R. Wurm and H. Frey, *Chem. Rev.*, 2016, **116**, 2170–2243.
24 A. Thomas, S. S. Müller and H. Frey, *Biomacromolecules*, 2014, **15**, 1935–1954.
25 J. Herzberger, K. Fischer, D. Leibig, M. Bros, R. Thiermann and H. Frey, *J. Am. Chem. Soc.*, 2016, **138**, 9212–9223.
26 S. Son, E. Shin and B.-S. Kim, *Macromolecules*, 2015, **48**, 600–609.
27 K. Niederer, C. Schüll, D. Leibig, T. Johann and H. Frey, *Macromolecules*, 2016, **49**, 1655–1665.
28 C. Tonhauser, A. Alkan, M. Schömer, C. Dingels, S. Ritz, V. Mailänder, H. Frey and F. R. Wurm, *Macromolecules*, 2013, **46**, 647–655.
29 J. Song, L. Palanikumar, Y. Choi, I. Kim, T. Heo, E. Ahn, S.-H. Choi, E. Lee, Y. Shibasaki, J.-H. Ryu and B.-S. Kim, *Polym. Chem.*, 2017, **8**, 7119–7132.
30 G. Ahn, S. Kweon, C. Yang, J. E. Hwang, K. Kim and B.-S. Kim, *J. Polym. Sci., Part A: Polym. Chem.*, 2017, **55**, 4013–4019.
31 J. Zhang and G. Wang, *Sci. China: Chem.*, 2015, **58**, 1674–1694.
32 X. Song, M. Cao, P. Chen, R. Xia, Z. Zheng, J. Miao, B. Yang, L. Su, J. Qian and X. Feng, *Polym. Bull.*, 2017, **74**, 183–194.

33 Y. Oikawa, S. Lee, D. H. Kim, D. H. Kang, B.-S. Kim, K. Saito, S. Sasaki, Y. Oishi and Y. Shibasaki, *Biomacromolecules*, 2013, **14**, 2171–2178.
34 P. Olsén, T. Borke, K. Odelius and A.-C. Albertsson, *Biomacromolecules*, 2013, **14**, 2883–2890.
35 M. Siebert, H. Keul and M. Möller, *Des. Monomers Polym.*, 2010, **13**, 547–563.
36 B. Zhang, Y. Ma, D. Chen, J. Xu and W. Yang, *J. Appl. Polym. Sci.*, 2013, **129**, 113–120.
37 E. R. Moore, *Ind. Eng. Chem. Prod. Res. Dev.*, 1986, **25**, 315–321.
38 B. S. Beckingham, G. E. Sanoja and N. A. Lynd, *Macromolecules*, 2015, **48**, 6922–6930.
39 M. Wilhelm, C. Le Zhao, Y. Wang, R. Xu, M. A. Winnik, J. L. Mura, G. Riess and M. D. Croucher, *Macromolecules*, 1991, **24**, 1033–1040.
40 F. K. Wolf, A. M. Hofmann and H. Frey, *Macromolecules*, 2010, **43**, 3314–3324.
41 T. Noda, A. Hashidzume and Y. Morishima, *Macromolecules*, 2001, **34**, 1308–1317.
42 S. Stolnik, L. Illum and S. S. Davis, *Adv. Drug Delivery Rev.*, 1995, **16**, 195–214.
43 T. Isono, K. Miyachi, Y. Satoh, S. Sato, T. Kakuchi and T. Satoh, *Polym. Chem.*, 2017, **8**, 5698–5707.
44 M. D. McCluskey, D. I. Grover and K. K. Zhuravlev, *Chem. Lett.*, 2002, **31**, 1138–1139.
45 M. Worm, D. Leibig, C. Dingels and H. Frey, *ACS Macro Lett.*, 2016, **5**, 1357–1363.
46 C. Tonhauser, C. Schüll, C. Dingels and H. Frey, *ACS Macro Lett.*, 2012, **1**, 1094–1097.
47 E. S. Lee, K. Na and Y. H. Bae, *Nano Lett.*, 2005, **5**, 325–329.
48 X. Zhang, Y. Huang, M. Ghazwani, P. Zhang, J. Li, S. H. Thorne and S. Li, *ACS Macro Lett.*, 2015, **4**, 620–623.
49 R. Duncan and S. C. W. Richardson, *Mol. Pharm.*, 2012, **9**, 2380–2402.
50 S. D. Conner and S. L. Schmid, *Nature*, 2003, **422**, 37–44.
51 J. Lu, S. C. Owen and M. S. Shoichet, *Macromolecules*, 2011, **44**, 6002–6008.
52 S. Jiwpanich, J.-H. Ryu, S. Bickerton and S. Thayumanavan, *J. Am. Chem. Soc.*, 2010, **132**, 10683–10685.
53 J.-H. Ryu, R. T. Chacko, S. Jiwpanich, S. Bickerton, R. P. Babu and S. Thayumanavan, *J. Am. Chem. Soc.*, 2010, **132**, 17227–17235.
54 L. Li, J.-H. Ryu and S. Thayumanavan, *Langmuir*, 2013, **29**, 50–55.
55 Y. Xia, J. Shen, H. Alamri, N. Hadjichristidis, J. Zhao, Y. Wang and G. Zhang, *Biomacromolecules*, 2017, **18**, 3233–3237.
56 S.-H. Choi, F. S. Bates and T. P. Lodge, *J. Phys. Chem. B*, 2009, **113**, 13840–13848.